Multistate Photo-Induced Relaxation and Photoisomerization Ability of Fumaramide Threads: A Computational and Experimental Study

ARTICLE *in* JOURNAL OF THE AMERICAN CHEMICAL SOCIETY · JANUARY 2009

Impact Factor: 12.11 · DOI: 10.1021/ja802531j · Source: PubMed

14 AUTHORS, INCLUDING:

Piero Altoè
E4 Computer Engineering
34 PUBLICATIONS **709** CITATIONS
SEE PROFILE

Albert M Brouwer
University of Amsterdam
142 PUBLICATIONS **3,412** CITATIONS
SEE PROFILE

Grzegorz Balkowski
8 PUBLICATIONS **56** CITATIONS
SEE PROFILE

J|A|C|S ARTICLES

Published on Web 12/15/2008

Multistate Photo-Induced Relaxation and Photoisomerization Ability of Fumaramide Threads: A Computational and Experimental Study

Piero Altoè,[†] Natalia Haraszkiewicz,[‡,§] Francesco G. Gatti,[II,⊥] Piet G. Wiering,[‡] Céline Frochot,[‡,∫] Albert M. Brouwer,[‡] Grzegorz Balkowski,[‡,¶] Daniel Shaw,[‡] Sander Woutersen,[‡] Wybren Jan Buma,[‡] Francesco Zerbetto,[†] Giorgio Orlandi,[†] David A. Leigh,[II] and Marco Garavelli*[,†]

Dipartimento di Chimica "G.Ciamician", Università di Bologna, via Selmi 2, 40126 Bologna, Italy, Van't Hoff Institute for Molecular Sciences, University of Amsterdam, Nieuwe Achtergracht 166, 1018 WV Amsterdam, The Netherlands, and School of Chemistry, University of Edinburgh, The King's Buildings, West Mains Road, Edinburgh, EH9 3JJ, United Kingdom

Received April 7, 2008; E-mail: marco.garavelli@unibo.it

Abstract: Fumaric and maleic amides are the photoactive units of an important and widely investigated class of photocontrollable rotaxanes as they trigger ring shuttling via a cis−trans photoisomerization. Here, ultrafast decay and photoinduced isomerization in isolated fumaramide and solvated nitrogen-substituted fumaramides (that are employed as threads in those rotaxanes) have been investigated by means of CASPT2//CASSCF computational and time-resolved spectroscopic techniques, respectively. A complex multistate network of competitive deactivation channels, involving both internal conversion and intersystem crossing (ISC) processes, has been detected and characterized that accounts for the picosecond decay and photochemical/photophysical properties observed in the singlet as well as triplet (photosensitized) photochemistry of fumaramides threads. Interestingly, singlet photochemistry appears to follow a non-Kasha rule model, where nonequilibrium dynamical factors control the outcome of the photochemical process: accessible high energy portions of extended crossing seams turn out to drive the deactivation process and ground-state recovery. Concurrently, extended singlet/triplet degenerate regions of twisted molecular structures with significant spin−orbit-coupling values account for ultrafast (picosecond time scale) ISC processes that lead to higher photoisomerization efficiencies. This model discloses the principles behind the intrinsic photochemical reactivity of fumaramide and its control.

1. Introduction

Control of large amplitude submolecular movements is a prerequisite for the development of artificial devices that function through motion at the molecular level. Large amplitude internal translation can be induced by different types of stimuli: acid base reaction,[1−3] redox reaction[4−8] and light absorption,[6,9−13] which are an inherent characteristic of many catenanes and rotaxanes.[14,15]

Fumaramide motifs template the assembly of benzylic amide macrocycles (called *rings*) around them (called *threads*) to form

[†] Università di Bologna.
[‡] University of Amsterdam.
[§] Present address: Biotechnology Department, Synthon BV Microweg 22, 6503 GN Nijmegen, The Netherlands.
[II] University of Edinburgh.
[⊥] Present address: Dipartimento di Chimica, Materiali e Ingegneria Chimica "Giulio Natta", Politecnico di Milano, Via Mancinelli 7, 20131 Milano, Italy.
[∫] Present address: DCPR, Nancy-University, CNRS, 1 rue Grandville BP 20451 F-54001, Nancy, France.
[¶] Present address: Institute of Inorganic Technology and Mineral Fertilizers, Wrocław University of Technology, ul. Smoluchowskiego 25, 50-372 Wrocław, Poland.

(1) Bissell, R. A.; Cordova, E.; Kaifer, A. E.; Stoddart, J. F. *Nature* **1994**, *369*, 133.
(2) Badjic, J. D.; Balzani, V.; Credi, A.; Silvi, S.; Stoddart, J. F. *Science* **2004**, *303*, 1845.
(3) Keaveney, C. M.; Leigh, D. A. *Angew. Chem., Int. Ed.* **2004**, *43*, 1222.
(4) Tseng, H.-R.; Vignon, S. A.; Stoddart, J. F. *Angew. Chem., Int. Ed.* **2003**, *42*, 1491.
(5) Altieri, A.; Gatti, F. G.; Kay, E. R.; Leigh, D. A.; Martel, D.; Paolucci, F.; Slawin, A. M. Z.; Wong, J. K. Y. *J. Am. Chem. Soc.* **2003**, *125*, 8644.
(6) Brouwer, A. M.; Frochot, C.; Gatti, F.; Leigh, D. A.; Mottier, L.; Paolucci, F.; Roffia, S.; Wurpel, G. W. H. *Science* **2001**, *291*, 2124.
(7) Fioravanti, G.; Haraszkiewicz, N.; Kay, E. R.; Mendoza, S. M.; Bruno, C.; Marcaccio, M.; Wiering, P. G.; Paolucci, F.; Rudolf, P.; Brouwer, A. M.; Leigh, D. A. *J. Am. Chem. Soc.* **2008**, *130*, 2593.
(8) Jagesar, D. C.; Hartl, F.; Buma, W. J.; Brouwer, A. M. *Chem.−Eur. J.* **2008**, *14*, 1935.
(9) Murakami, H.; Kawabuchi, A.; Kotoo, K.; Kunitake, M.; Nakashima, N. *J. Am. Chem. Soc.* **1997**, *119*, 7605.
(10) Stanier, C. A.; Alderman, S. J.; Claridge, T. D. W.; Anderson, H. L. *Angew. Chem., Int. Ed.* **2002**, *41*, 1769.
(11) Altieri, A.; Bottari, G.; Dehez, F.; Leigh, D. A.; Wong, J. K. Y.; Zerbetto, F. *Angew. Chem., Int. Ed.* **2003**, *42*, 2296.
(12) Balzani, V.; Clemente-Leon, M.; Credi, A.; Ferrer, B.; Venturi, M.; Flood, A. H.; Stoddart, J. F. *Proc. Natl. Acad. Sci. U.S.A.* **2006**, *103*, 1178.
(13) Leigh, D. A.; Morales, M. Á. F.; Pérez, E. M.; Wong, J. K. Y.; Slawin, A. M. Z.; Carmichael, A. J.; Haddleton, D. M.; Brouwer, A. M.; Buma, W. J.; Wurpel, G. W. H.; León, S.; Zerbetto, F. *Angew. Chem., Int. Ed.* **2005**, *44*, 3062.

10.1021/ja802531j CCC: $40.75

Scheme 1[a]

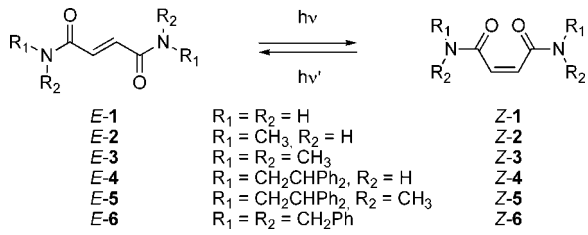

E-**1**	$R_1 = R_2 = H$	*Z*-**1**
E-**2**	$R_1 = CH_3$, $R_2 = H$	*Z*-**2**
E-**3**	$R_1 = R_2 = CH_3$	*Z*-**3**
E-**4**	$R_1 = CH_2CHPh_2$, $R_2 = H$	*Z*-**4**
E-**5**	$R_1 = CH_2CHPh_2$, $R_2 = CH_3$	*Z*-**5**
E-**6**	$R_1 = R_2 = CH_2Ph$	*Z*-**6**

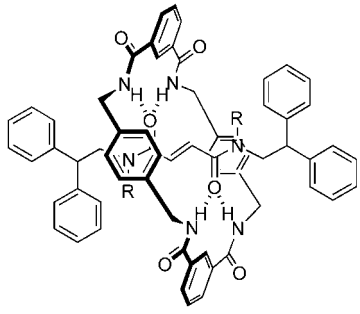

7 R = H
8 R = CH_3

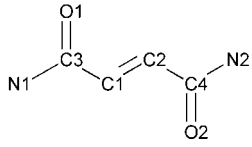

[a] Investigated fumaramide/maleamide compounds and their photoinduced isomerization (top). The structural formula of a very simple fumaramide based rotaxane (middle) and the atoms numbering used in the text are also displayed (bottom).

rotaxanes in high yields[16] (see Scheme 1). The fumaramide unit (that is also referred to as a *station* of the thread) also provides an opportunity to enforce a geometrical change in the thread after rotaxane formation. In fact, isomerization of the olefin from *E* to *Z*, triggered photochemically, disrupts the near-ideal hydrogen bonding structure between macrocycle and thread and changes the internal dynamics governed by those interactions (such as the shuttling of the ring along the thread). The photoisomerization interconverts fumaramide (trans) and maleamide (cis) isomers of the olefinic unit. The trans olefin holds its two strongly hydrogen bond accepting amide carbonyl groups in a preorganized close-to-ideal spatial arrangement for interaction with the amide groups of the macrocycle. Photoisomerization reduces the number of possible intercomponent hydrogen bonds at the olefin station from four to two and the macrocycle can change position to another station, if present, that is essentially indefinitely stable until a further stimulus is applied to reisomerize the maleamide unit back to fumaramide. The switching process is reversible: subjecting the maleamide rotaxanes to heat, or a suitable catalyst, or a second photon of different wavelength, results in reisomerization to the more thermally stable trans-olefin isomers, with accompanying reinstatement of the strong hydrogen-bonding network. As long as photons of a suitable wavelength are supplied, the process will continue indefinitely, apart from losses due to side reactions and fatigue effects.

To access the details of this photoinduced process, a computational study of the photochemical isomerization and multistate relaxation channels of the bare photoactive unit (i.e., the unsubstituted fumaramide *E*-**1**) has been performed *in vacuo*, jointly with photochemical and spectroscopic measurements (including time-resolved subpicosecond time scale experiments) on *N*,*N*′- and *N*,*N*′*N*′-substituted fumaramides/maleamides (**2**−**6**) in dichloromethane/methanol or acetonitrile solution. Specifically, a high level CASPT2//CASSCF state-of-the-art quantum mechanical description[17] of the chemical system has been used to map the relevant photochemical channels and deactivation routes of isolated *E*-**1**, which has been used as a model system for the photochemical reactivity of fumaramides threads (*E*-**4**, *E*-**5** and *E*-**6**). Then, recorded time-resolved observations have been compared/combined to these computational results to provide a full rationale of fumaramide photochemical activity. Eventually, the purpose is to unveil the factors that control the photoinduced dynamics of this chromophore, so that our ability to understand, predict and control its behavior may be increased. It is also apparent that this information may turn out to be useful for a more efficient use of these systems in fumaramide-based rotaxanes (**7**,**8**).[18]

This work adds to the in depth studied field of alkene photoisomerizations: despite the existing extended (both experimental and theoretical) literature (spanning from neutral to polar conjugated organic molecules such as carotenes, retinals, stilbenes/azobenzenes/diarylethenes and their analogs, coumaric acid derivatives, etc) that has been widely reviewed both in the past and more recent times (see refs 19−23), to the best of our knowledge, the photochemistry of fumaric amides has never been investigated computationally before. Fumaric esters were studied in the seminal paper by Hammond,[24] while acroleine photochemistry (a rough precursor of the investigated systems that, although lacking the amide bond, has similar $n\rightarrow\pi^*/\pi\rightarrow\pi^*$ excited states) has also been documented (see ref 25). The fumaramide photochemistry will be shown to be unique and drastically different (and far more complex) than the one reported for apparently similar conjugated molecules, such as hexatrienes, acroleines, etc. In this respect, the work is theoretically valuable by itself as it delivers a novel information on a system that is a prototypical photoactive molecule with promising (nanotechnological) applications.

2. Computational and Experimental Details

2.1. Computational Section. Fumaramide *E*-**1** (a small molecule of 14 atoms that can be studied at a high *ab initio* level) has been

(14) Balzani, V.; Credi, A.; Raymo, F. M.; Stoddart, J. F. *Angew. Chem., Int. Ed.* **2000**, *39*, 3348.
(15) Barbara, P. F. *Acc. Chem. Res.* **2001**, *34*, 409.
(16) Gatti, F. G.; Leigh, D. A.; Nepogodiev, S. A.; Slawin, A. M. Z.; Teat, S. J.; Wong, J. K. Y. *J. Am. Chem. Soc.* **2001**, *123*, 5983.
(17) Andersson, K.; Malmqvist, P. A.; Roos, B. O.; Sadlej, A. J.; Wolinski, K. *J. Phys. Chem.* **1990**, *94*, 5483.
(18) Gatti, F. G.; Leon, S.; Wong, J. K. Y.; Bottari, G.; Altieri, A.; Morales, M. A. F.; Teat, S. J.; Frochot, C.; Leigh, D. A.; Brouwer, A. M.; Zerbetto, F. *Proc. Natl. Acad. Sci. U.S.A.* **2003**, *100*, 10.
(19) Altoe′, P.; Bernardi, F.; Conti, I.; Garavelli, M.; Negri, F.; Orlandi, G. *Theor. Chem. Acc.* **2007**, *17*, 1041.
(20) Gilbert, A.; Baggott, J. *Essentials of Molecular Photochemistry*; Blackwell Science: Oxford, 1991.
(21) Horspool, W. M.; Song, P.-S. *CRC Handbook of Organic Photochemistry and Photobiology*; CRC Press: Boca Raton, FL, 1995.
(22) Klessinger, M.; Michl, J. *Excited States and Photochemistry of Organic Molecules*; VCH Publishers: New York, 1994.
(23) Michl, J.; Bonacic-Koutecky, V. *Electronic Aspects of Organic Photochemistry*; Wiley & Sons, Inc.: New York, 1990.
(24) Hammond, G. S.; Saltiel, J.; Lamola, A. A.; Turro, N. J.; Bradshaw, J. S.; Cowan, D. O.; Counsell, R. C.; Vogt, V.; Dalton, C. *J. Am. Chem. Soc.* **1964**, *86*, 3197.
(25) Reguero, M.; Olivucci, M.; Bernardi, F.; Robb, M. A. *J. Am. Chem. Soc.* **1994**, *116*, 2103.

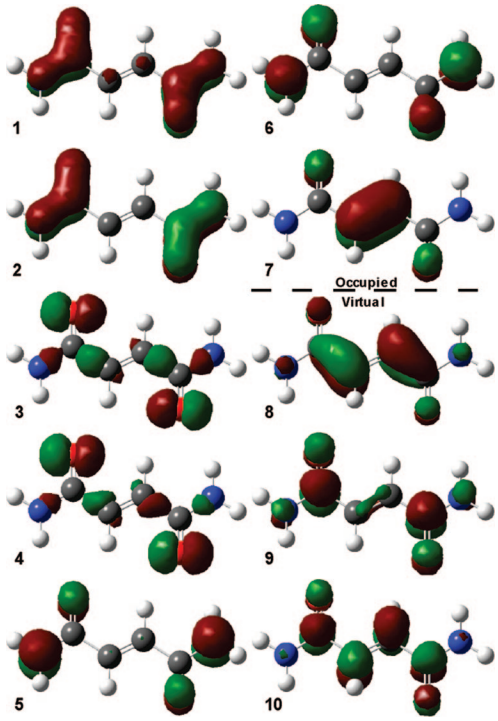

Figure 1. Fumaramide active space MOs.

selected as a model of the fumaramide thread *E*-**4** (see Scheme 1). A complete active space-self-consistent field (CASSCF)/6−31G* level of theory has been adopted for all geometry optimizations and minimum energy paths (MEP) computations, using the tools available in the Gaussian98 suite of programs.[26] For this purpose, a full active space of 14 electrons in 10 orbitals (i.e., all the p orbitals/electrons of the molecule plus the two *p* lone pairs on the oxygen atoms, see Figure 1) has been used. A state average procedure has also been employed, equally weighting the investigated root (for which the gradient is computed) and all the lower lying states.

MEPs have been computed by following the prescriptions described in refs 27 and 28. Briefly, to locate the relaxation channels (i.e., the MEPs) departing from the lower tip of a conical intersection point or the FC region, an initial direction of relaxation (IRD) (as close as possible to the conical intersection/FC point) has been located, and then a standard fully unconstrained MEP computation following that IRD has been computed in mass weighted coordinates.

To improve the energy profiles along the computed MEPs, single point multiconfigurational second-order perturbation theory computations have been carried out to account for correlation effects, using the complete active space second-order perturbation theory (CASPT2) method[17] implemented in MOLCAS 5.[29] To minimize the influence of weakly interacting intruder states the so-called imaginary level-shift technique was employed[30] (an imaginary level-shift value of 0.1 has been used throughout all the calculations, which was selected by a calibration procedure and found to produce stable results). A 5 roots state average procedure and an *ano-s* (10s6p3d/*3s2p1d*)[31] basis set have been employed. This strategy (i.e., CASSCF geometry optimizations plus single point CASPT2 energy corrections on top of these structures) is referred to as a CASPT2//CASSCF approach. All these computations have been performed *in vacuo*.

Table 1. Molar Absorption Coefficients at the Absorption Maxima and at 254 nm (Irradiation Wavelength) of the Compounds Studied Experimentally

Compound	λ_{max} (nm)	ϵ (λ_{max}) ($M^{-1}cm^{-1}$)	ϵ (λ_{254nm}) ($M^{-1}cm^{-1}$)
E−**3**	265	−	−
E−**4**	250 (shoulder)	13500[a]	13200[a]
			14200[b]
E−**5**	264	7700[a]	7000[a]
			7600[b]
Z−**4**	250 (shoulder)	8700[a]	8600[b]
Z−**5**	250 (shoulder)	7000[a]	7500[b]

[a] acetonitrile. [b] dichloromethane.

2.2. Experimental Section. Synthesis. The synthesis of threads were performed as described previously.[18] Suitable threads were prepared in a single step from fumaryl chloride (*E*-**4**, *E*-**5**) or maleic acid (*Z*-**4**) and a bulky primary (**4**) or secondary amine (**5**). N-methylated thread *Z*-**5** was conveniently obtained from *E*-**5** upon sensitized isomerization by 350 nm irradiation in the presence of benzophenone as a sensitizer, followed by separation from the benzophenone, and small amounts of photobyproducts, on a silicagel column using $CHCl_3$/EtOAc as the eluent. *E*-**3** was prepared as described by Montaudo et al. [32]

Spectroscopy. Steady state absorption spectra were recorded on a Cary 3 (Varian) spectrometer. The details of the setup employed for the femtosecond transient absorption experiments have been reported before.[33] Briefly, a Hurricane (Spectra Physics) laser/amplifier system generated a pulse train (130 fs fwhm, 800 nm center wavelength, 1 kHz repetition rate) that was separated into two parts. One part was employed to pump an Optical Parametric Amplifier, which generated pump pulses at 270 nm, the other part was focused on a calcium fluoride crystal to generate a white light continuum from 350 to 800 nm used for the probe pulse. The polarizations of the two beams were set at the magic angle. The probe beam was coupled into a 400 μm optical fiber after passing the sample and was detected with a CCD spectrometer (Ocean Optics, PC 2000). A chopper (Rofin Ltd., 83 Hz) placed in the excitation beam provided I and I_0 depending on the status of the chopper (open or closed). The total instrumental response was about 200 fs (fwhm). The excitation power was kept as low as ~5 μJ per pulse using a pump spot diameter of about 1 mm. Apart from using a relatively low excitation intensity, thermal effects and photodegradation were also taken care of by stirring the solution. Photodegradation was not substantial as shown by comparing absorption spectra taken before and after the transient absorption experiment. All experiments were performed at ambient temperature.

Details of the photochemical experiments are given in the Supporting Information.

3. Results and Discussion

The interplay between the potential energy surfaces (PESs) of the photochemically relevant electronic states is rather complicated. Two different and alternative interpretative models (thereafter called as the *static* and *dynamics* view) will be presented, discussed and compared with the experimental data documented here. All the (experimental and computational) results have been collected in Tables 1−4 and are presented in Figures 2[XI]−13, including a schematic (cartoon like) representa-

(26) Frisch, M. J.; et al. *Gaussian 98*, revision A.6; Gaussian Inc.: Pittsburgh PA, 1998.
(27) Bearpark, M. J.; Robb, M. A.; Schlegel, H. B. *Chem. Phys. Lett.* **1994**, *223*, 269.
(28) Celani, P.; Robb, M. A.; Garavelli, M.; Bernardi, F.; Olivucci, M. *Chem. Phys. Lett.* **1995**, *243*, 1.
(29) Andersson, K.; et al. *MOLCAS*, Version 5.4; Lund University: Sweden, 2002.
(30) Forsberg, N.; Malmqvist, P.-A. *Chem. Phys. Lett.* **1997**, *274*, 196.
(31) Widmark, P.-O.; Persson, B. J.; Roos, B. O. *Theor. Chem. Acc.* **1991**, *79*, 419.
(32) Montaudo, G.; Maravigna, P.; Caccamese, S.; Librando, V. *J. Org. Chem.* **1974**, *39*, 2806.
(33) Balkowski, G.; Szemik-Hojniak, A.; vanStokkum, I. H. M.; Zhang, H.; Buma, W. J. *J. Phys. Chem. A* **2005**, *109*, 3535.

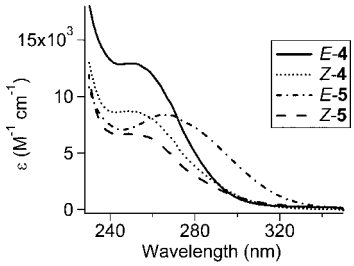

Figure 2. UV absorption spectra in dichloromethane.

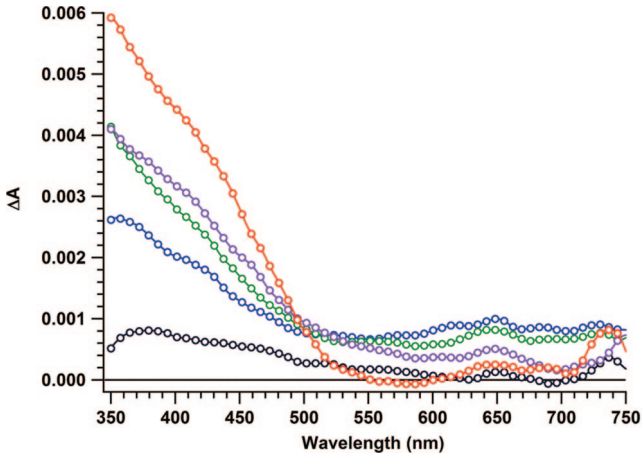

Figure 3. Transient absorption spectra of E-**4** upon excitation using 100 fs pulses of 275 nm and 1 μJ pulse energy. The spectral data depicted represent the excited-state history at times of 0.7 ps, (red) 1 ps, (violet) 1.3 ps, (green) 2.0 ps (blue) and 20 ps (black) after photoexcitation.

tion of the potential energy surfaces involved in the two (*static* and *dynamics*) models (Figures 7 and 10, respectively).

3.1. Absorption Spectra: The Singlet Manifold. Experiments. The spectroscopic data for threads **4** and **5** are gathered in Table 1. The spectra (Figure 2) are characterized by a strong absorption band at ca. 250−260 nm, which appears as a shoulder on a stronger band at shorter wavelength. Based on a comparison with other substituted alkenes we can attribute the absorption bands to $\pi\rightarrow\pi$ * transitions.[34] Such transitions are known to possess high intensity. The molar absorption coefficient at the absorption maximum for the simple ethene chromophore is in the range of 10000 $M^{-1}cm^{-1}$, but it depends strongly on substituents. The molar absorption coefficient is higher for *E*-**4**, ca. 14000 $M^{-1}cm^{-1}$, but it is lower for *E*-**5** (ca. 7000 $M^{-1}cm^{-1}$). The absorption maximum for *E*-**5**, on the other hand, occurs at a longer wavelength. The substituents on the nitrogen atoms have a substantial influence on the transitions of the chromophore because they affect the relative energies of the p-basis orbitals contributing to the π -MOs. The molar absorption coefficients for *Z*-isomers are generally lower than those of the corresponding *E*-isomers because the chromophore is less extended. For the case of *Z*-**5**, the chromophore is nonplanar, which further contributes to a higher vertical excitation energy and smaller absorption coefficient. None of the compounds investigated shows detectable fluorescence. Therefore it is not possible to properly estimate the 0−0 excitation energy.

Calculations. The first two excited singlet states ($S_1(B_g)$ and $S_2(A_u)$) for fumaramide *E*-**1** are almost degenerate and are characterized by a single $n\rightarrow\pi^*$ electronic transition between the orbitals 3→8 and 4→8 (see Figure 1), respectively; while the next two higher energy ones ($S_3(B_u)$ and $S_4(A_g)$) are characterized by single $\pi\rightarrow\pi^*$ excitations. In particular, $S_3(B_u)$ is the bright state (oscillator strength ∼0.1), which absorbs at 239 nm (see Table 2) and is mainly described by a single excitation between the orbitals 7 and 8 (that are located respectively on the C═C central bond (*C1*−*C2*) and the adjacent (*C1*−*C3*, *C2*−*C4*) bonds, see Figure 1. Note that this value is close to the experimental maxima recorded for the UV/vis spectrum of the threads *E*-**4** and *E*-**5** in CH_2Cl_2 (250 and 264 nm respectively, see Table 1 and Figure 2). The red shift recorded for the thread absorption maximum (as compared to the computed value of the parent unsubstituted fumaramide compound *E*-**1**) can be attributed to the hyperconjugative effect of the alkyl substituents. In fact, similar computations on *E*-**2** (251 nm, see Table 2) and *E*-**3** (277 nm, see Table 2), that can be regarded as model compounds for *E*-**4** and *E*-**5**, do nicely reproduce the experimental values for *E*-**4** and *E*-**5**, respectively. Even considering the broad maximum region of the recorded solution spectra (see Figure 2), the agreement between computations (that have been performed in isolated conditions) and experiments is remarkably good. As our computations in vacuo reproduce the spectroscopic data recorded in solution, we think that solvent effects may be considered negligible in this specific case and that the isolated system models the photochemical behavior in solution.

3.2. E⇆Z Photochemical Isomerization. Direct Irradiation Experiments. *E* and *Z*-isomers are separable and stable in their ground states. Thus, it is straightforward to determine by conventional analytical methods the ratio of the two isomers at the photostationary state as well as the isomerization quantum yields. Since the absorption spectra of *E* and *Z*-isomer pairs of threads are quite similar, they are not suitable for accurately determining the concentration changes following irradiation. For the same reason they cannot be used to calculate the ratio of isomers at the photostationary state, which is, in contrast, possible in the case of many stilbene analogs or azobenzene analogs described in the literature.[9,35−37] Instead, ^{1}H NMR (the chemical shifts of protons at the double bonds or protons from NH groups are different in case of *E* and Z-isomers) or the more sensitive HPLC method were applied to determine the isomer ratios.

Photostationary States. Photoisomerization upon 254 or 300 nm irradiation is reversible and after a period of exposure, typically 30 min. to 1 h, depending on conditions, a photostationary *E*-*Z* equilibrium is attained, where the ratio of both isomers does not change after further prolongation of the irradiation. The results of these irradiation experiments are summarized in Table 3. Since UV absorbance of *Z*-isomers is lower than that of *E*-isomers, it is not surprising that the photostationary states consist of only 38% and 16% of the initial *E*-isomers for the pairs of *E*-**4**/*Z*-**4**, and *E*-**5**/*Z*-**5**, respectively. Quite similar values were obtained by analyzing the mixture of isomers with ^{1}H NMR and HPLC. The ratio of *E* and *Z*-isomers at the photostationary state depends on the excitation wavelengths but the differences are not large.

Photoisomerization Quantum Yields. Quantum yields of photoisomerizations of **4** and **5** in acetonitrile were measured

(34) Hesse, M.; Meier, H.; Zeeh, B. *Spectroscopic Methods in Organic Chemistry*, 2nd ed.; Georg Thieme Verlag: Stuttgart, Germany, 2008.

(35) Bortolus, P.; Monti, S. *J. Phys. Chem.* **1979**, *83*, 648.
(36) Birnbaum, P. P.; Style, D. W. G. *Trans. Faraday Soc.* **1954**, *50*, 1192.
(37) Siampiringue, N.; Guyot, G.; Monti, S.; Bortolus, P. *J. Photochem.* **1987**, *37*, 185.

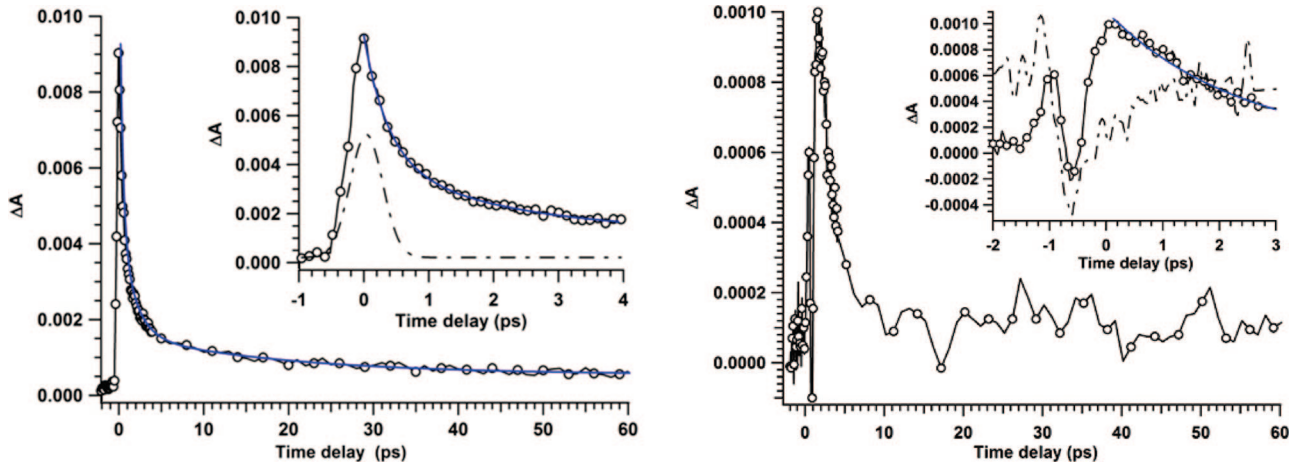

Figure 4. Left: The decay profile for *E*-**4** monitored at 375 nm over a 60 ps time scale, with in the insert the decay for short pump−probe delays. The solvent response (dashed/dotted line in the insert) was experimentally determined from the excitation of a sample containing exclusively the solvent. The blue line is a biexponential fit with lifetimes of 1.7 ± 0.2 and 19 ± 1 ps obtained after deconvolution of the decay with the solvent response. Right: The decay profile for *E*-**4** monitored at 650 nm with in the insert the decay for short pump−probe delays and the solvent response. The blue line derives from a monoexponential fit with a lifetime of 1.7 ps.

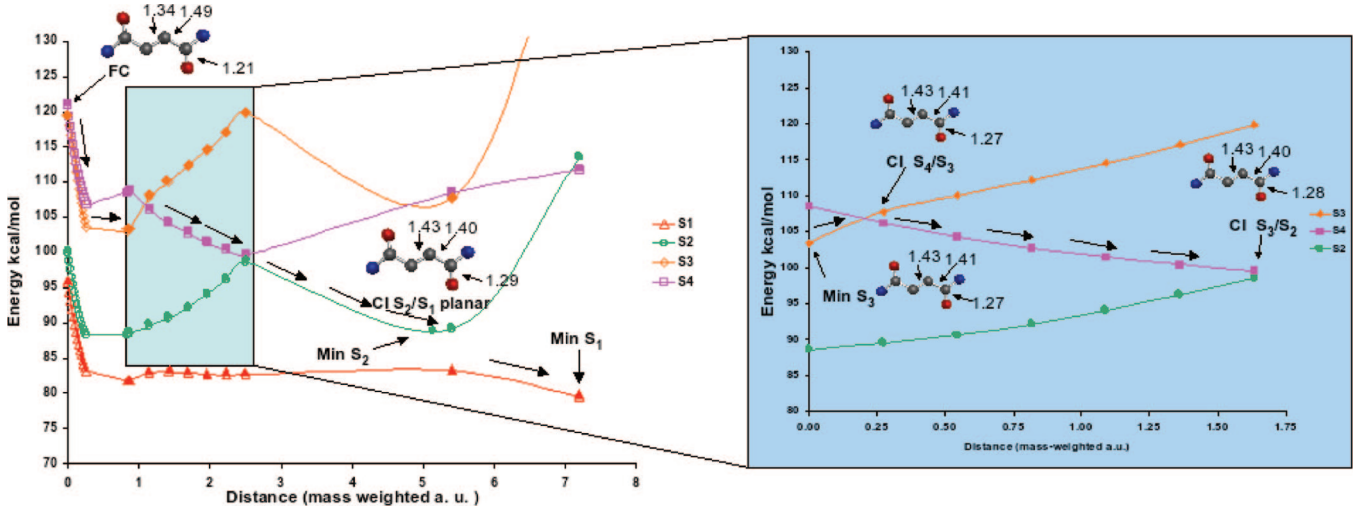

Figure 5. Deactivation paths (MEPs) for fumaramide *E*-**1** from the $S_3(\pi\pi^*)$ Franck−Condon point to the minimum on $S_1(n\pi^*)$. All energy values are calculated at the CASPT2/ano-s level (filled symbols) or at the CASSCF/ano-s level (empty symbols), which have been scaled to match the energies computed at the CASPT2/ano-s level.

by monitoring the conversion starting from each of the pure isomers using HPLC. The total conversion was kept small, so that corrections for the reverse reaction (excitation of the photoproduct) could be ignored. The concentrations of initial *E* and *Z*-isomers were ca. 1 mM, the photon flux was determined using the photocyclization of 1,3-cycloheptadiene (CHD) as actinometer.[38] For details see Supporting Information. Results are reported in Table 3. The isomerization quantum yields and the photostationary state composition are related according to eq 1:

$$\frac{\phi_{E\rightarrow Z}}{\phi_{Z\rightarrow E}} = \frac{\varepsilon_Z}{\varepsilon_E} \times \frac{[Z]_{PPS}}{[E]_{PPS}} \qquad (1)$$

in which $[Z]_{PPS}/[E]_{PPS}$ is the ratio of *Z*-isomer to *E*-isomer at the photostationary state and ϵ_Z and ϵ_E are the molar absorption coefficients. This allows a consistency check, results of which are included in Table 3.

The efficiencies of the isomerization process of *E*-**4** → *Z*-**4** and *Z*-**4** → *E*-**4** are almost the same (ca. 4.4%). The photoisomerization process is somewhat less efficient for methylated threads *E*-**5** and *Z*-**5** than for *E*-**4** and *Z*-**4**. The quantum yield for the *Z*-**5** → *E*-**5** process is even smaller than that for *E*-**5** → *Z*-**5** (0.28% and 1.5%, respectively).

In general, the photoisomerization quantum yields are rather low. This means that the relaxation to the ground-state proceeds via nonproductive funnel, or that the relaxation on the ground-state surface is biased in favor of the reactant rather than the product.[39] The recorded quantum yields for *E*→*Z* and *Z*→*E* photoisomerization of the thread are collected in Table 3.

Time-Resolved Experiments. Figure 3 displays chirp-uncorrected transient absorption spectra of *E*-**4** dissolved in dichloromethane for various pump−probe delay times. For short delay times, the absorption spectrum is dominated by two absorption bands. The stronger one of these bands is the one in the 350−450 nm region and appears to have a maximum below

(38) Numao, N.; Hamada, T.; Yonemitsu, O. *Tetrahedron Lett.* **1977**, *18*, 1661.

(39) Merchan, M.; Serrano-Andres, L. *J. Am. Chem. Soc.* **2003**, *125*, 8108.

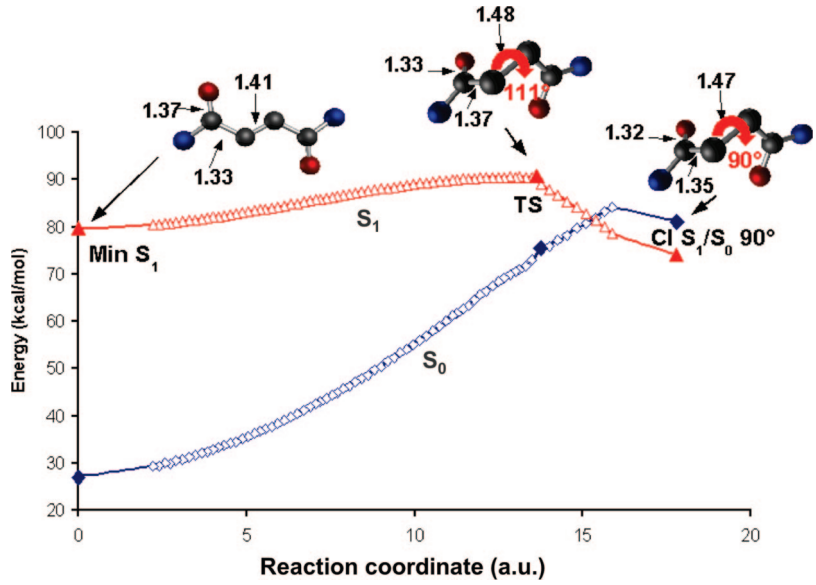

Figure 6. S_1 minimum energy path between the S_1 minimum (**Min S_1**) and the 90° twisted conical intersection (**CI S_1/S_0 90°**) computed for fumaramide *E*-**1**. Triangles and diamonds display the S_1 and S_0 energy profiles, respectively. All values are calculated at the CASSCF/ano-s level (empty symbols), which have been scaled to match the energies computed at the CASPT2/ano-s level (filled symbols). At CASPT2 level the conical intersection is anticipated, i.e. it is closer to the TS.

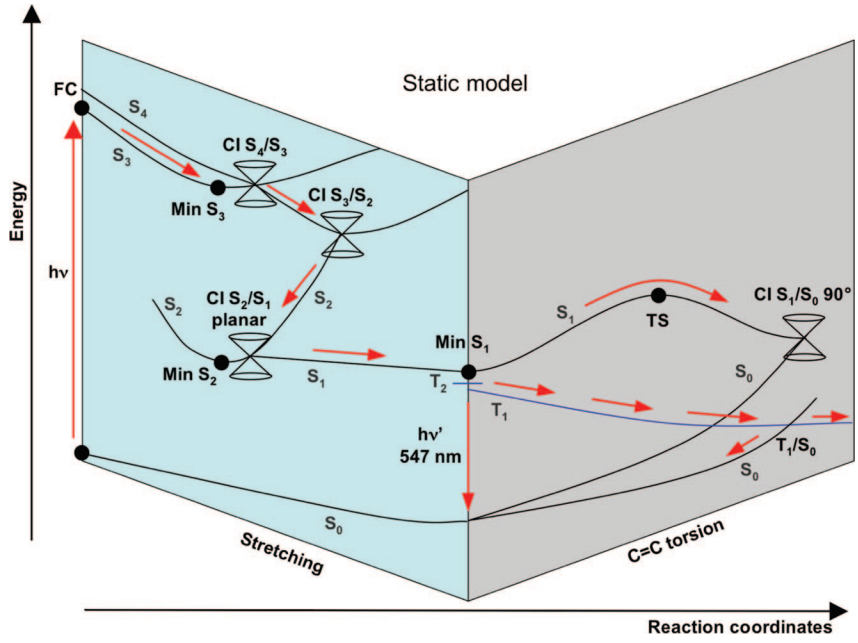

Figure 7. "Static interpretation" of fumaramide photochemistry.

350 nm, that is, outside the region covered by our white-light window. The other band in the 600−800 nm region is considerably weaker, but still distinctly present. For longer delay times, the latter band disappears and only a band with a maximum at ∼375 nm remains in the 350−500 nm region. Figure 4 shows decay traces taken at 375 and 650 nm. After deconvolution with the solvent response, the trace at 375 nm can be fit well with a biexponential decay with time constants of 1.7 ± 0.2 ps and 19 ± 1 ps. At 650 nm the solvent response precludes an accurate analysis of the trace below 1 ps, but for longer delay times the decay can be satisfactorily fitted with a monoexponential decay with a time constant of 1.7 ± 0.2 ps. Similar analyses have been performed for a range of wavelengths, and lead to the conclusion that the Decay Associated Difference Spectrum (DADS) of the fast component peaks at the aforementioned 350−450 and 600−800 nm bands, while that of the slow component is maximum around ∼375 nm and diminishes continuously for longer probe wavelengths.

The transient absorption spectra of the other systems, unfortunately, were of lower quality. However, analogously to the results on *E*-**4**, a rapid decay is observed for all molecules that—when fitted to a monoexponential decay—leads to decay times of 1.1 and 1.3 ps for *E*-**5** and *E*-**6**, respectively. It would thus appear that the primary excited-state dynamics are essentially the same in all cases.

The calculations and experimental absorption spectra leave no doubt that the initial excitation populates the $S_3(\pi\pi^*)$ state. Unfortunately, the solvent response at in particular the longer probe wavelengths do not allow us to observe processes faster than 300 fs, but we can safely assume that internal conversion

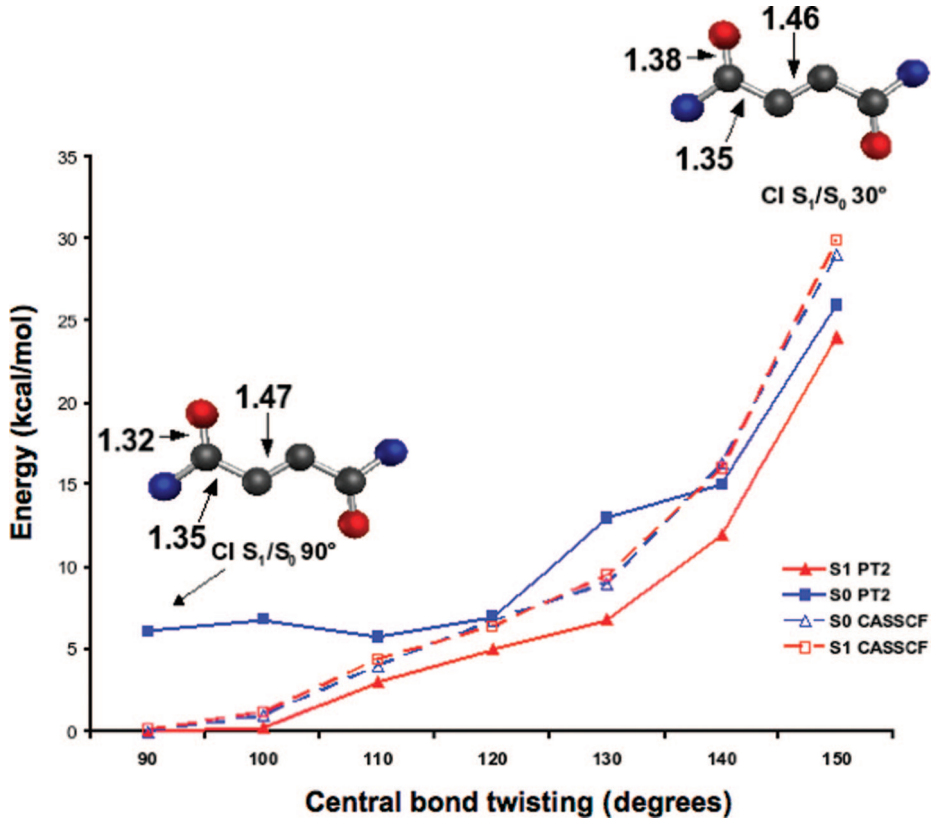

Figure 8. S_1/S_0 crossing seam computed for fumaramide *E*-**1**. Each point is obtained by constrained (at a fixed central bond dihedral angle) conical intersection optimization at the CASSCF level. Energies are re-evaluated at the CASPT2/6−31G* level: filled triangles and diamonds display the S_0 and S_1 CASPT2 corrected energy profiles, respectively. The blue line indicates the state diabatically connected to FC S_0, while the red line indicates the state diabatically connected to FC S_1. It is apparent here that the two states have already swapped at the CASPT2 level: as reported in Figure 6, the CASPT2 crossing region is displaced (i.e., anticipated) respect to the CASSCF one (dashed lines and empty symbols).

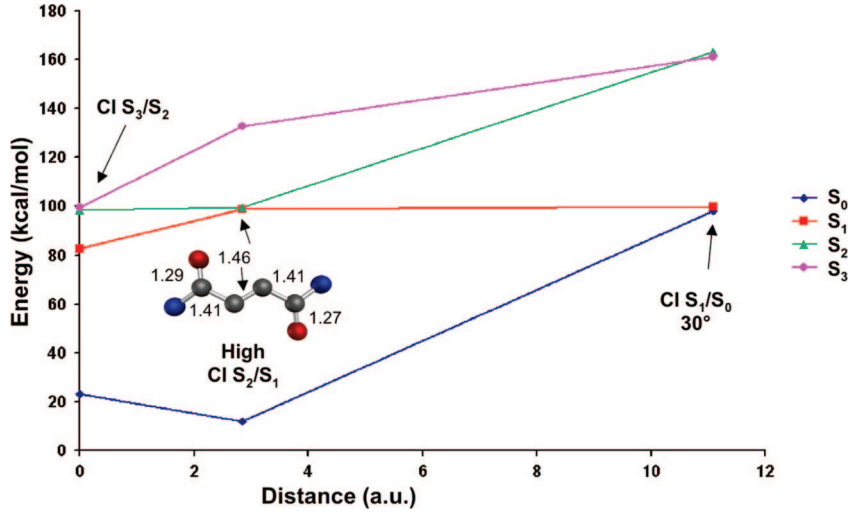

Figure 9. High energy S_3/S_2, S_2/S_1 and S_1/S_0 conical intersections (**CI S_3/S_2**, **High CI S_2/S_1** and **CI S_1/S_0 30°**, respectively) and their distance in mass weighted atomic units (a.u.). It is apparent that these points are isoenergetics and that **CI S_3/S_2** and **High CI S_2/S_1** are quite close each other.

of S_3 occurs faster than the first observable decay on the order of 0.5−1.7 ps. We therefore associate this decay component with the decay of another electronically excited state, most likely the S_1 state. For *E*-**4** a second decay component is observed. The absence of the 600−800 nm band at longer delay times indicates a change in the electronic character of the absorbing state. The steady-state absorption spectrum of *E*-**4** shows a lowest absorption band at 250 nm, and negligible absorption for wavelengths larger than 300 nm. This observation makes it unlikely that the ∼375 nm band observed for pump−probe delays larger than 10 ps is associated with absorption from a vibrationally hot ground state, and we therefore tentatively assign it to excited-state absorption from the T_1 state. Further support for such an assignment might be obtained by recording the transient absorption spectrum of T_1 generated, for example, by triplet sensitizers, but such experiments have not been

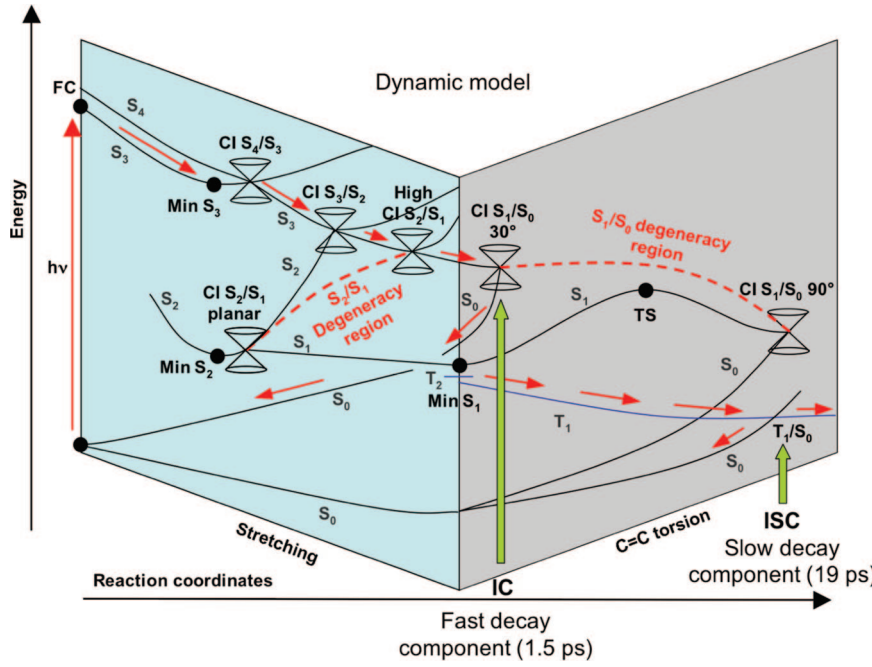

Figure 10. "Dynamic interpretation" of fumaramide photochemistry.

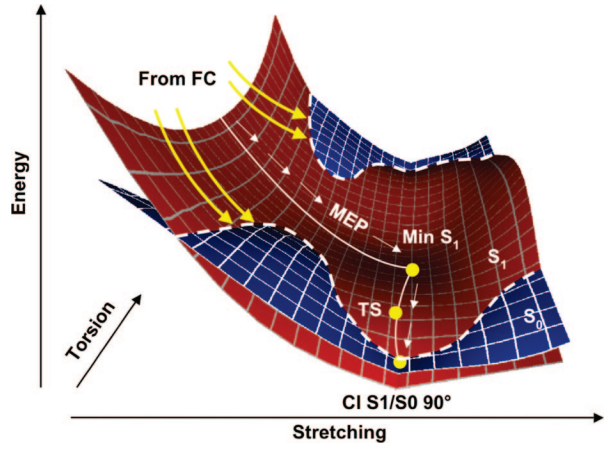

Figure 11. Cartoon representation for the *static* (short white arrows) and *dynamic* (long yellow arrows) models of fumaramide deactivation. The S_1/S_0 intersection space is represented by dashed lines.

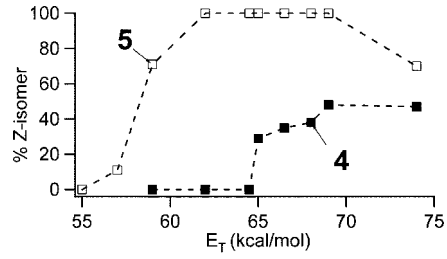

Figure 12. Conversion to the Z-isomers of **4** and **5** in acetonitrile after prolonged irradiation as a function of triplet sensitizer energy.

successful yet. Anyway, the computations documented below provide a further basis for this interpretation.

Finally, it is worth noting that the fumaric (trans) and maleic (cis) amides used in this work can adopt several low-energy conformations via rotations of the single bonds (C═C−C═O) and the amide bonds. This issue and the implications of isomers equilibria on the recorded experimental data are discussed in depth in section S1 of the Supporting Information.

Computational Analysis of Singlet Photochemistry: Static vs Dynamic Model. The results of CASPT2//CASSCF/6−31G* MEP mapping from the FC point of the first bright (S_3) $\pi\pi^*$ singlet state of *E*-**1** are summarized in Figures 5–7, while Tables 2 and 4 collect the relative energies and the structural data of all the relevant points discussed in the text, respectively. A first model for the photochemistry of the fumaramide unit has been formulated that is based only on the minimum energy points found (along the MEPs) on the potential energy surfaces of the photochemically relevant states. This mechanistic picture (which is schematically displayed and summarized in Figure 7) will be referred to in this paper as the *static model*.

In contrast to that picture, also the high energy regions of the photochemically relevant crossing seams have been investigated (see Figures 8−9). These regions are close to high energy portions of the computed MEPs and may be accessed dynamically if sufficient vibrational energy is available. They turn out to be important features for a realistic description of fumaramide photochemistry and a full understanding of the experimental results. The present analysis contributes to draw an alternative mechanistic picture that will be referred to in this paper as the *dynamic model* (and is schematically depicted in Figure 10).

(A) The Static Model. As pointed out in the subsection 3.1 above, direct photoexcitation promotes fumaramide to the spectroscopically allowed $\pi\rightarrow\pi^*$ $S_3(B_u)$ state. Relaxation from the Franck−Condon (FC) region of this state drives the system to a planar minimum (**Min S_3**) where the C_{2h} symmetry is preserved. A crossing point with the dark $\pi\rightarrow\pi^*$ $S_4(A_g)$ state (i.e., a **CI S_4/S_3** conical intersection) exists very close to the minimum region. The energy of this CI (2.7 kcal/mol above the minimum) has to be considered an upper limit because this crossing has been found through a linear

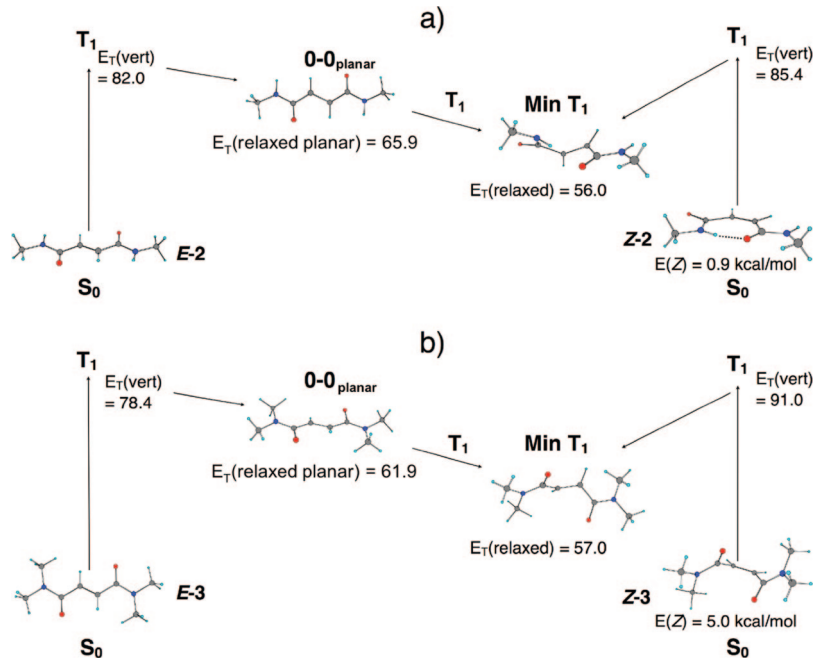

Figure 13. B3LYP/6−31G* calculations on **2** (a) and **3** (b) illustrating the different ground-state structures, associated vertical and adiabatic (0−0) triplet T_1 ($\pi\pi^*$) energies (energies values are relative to the *E* isomer ground state). The twisted minima on T_1 (**Min T_1**) and their relative energies have also been reported.

interpolation between the S_3 minimum and the **CI S_3/S_2** point (see below). After the conical intersection, the energy of S_3 (now the dark $\pi\rightarrow\pi^*$ state, diabatically connected to the FC $S_4(A_g)$ state) decreases until a new crossing is reached with the $n\rightarrow\pi^*$ S_2 state (**CI S_3/S_2**, see Figure 5). Interestingly, this motion (from FC to the **CI S_3/S_2**) only involves bond-stretching modes that preserve the planarity of the backbone, i.e. no double bond isomerization coordinates have yet been involved. Following decay through the first **CI S_3/S_2** crossing, it is conceivable that most of the molecules will be collected on the minimum of the $n\rightarrow\pi^*$ S_2 state (**Min S_2**), by relaxing on this surface (see Figure 5).

Again, the molecular deformations driving the system into this point do not involve C−C twisting motions but the rearrangement of the skeletal bond distances only. In particular, it turns out that by following the S_2 MEP from the **CI S_3/S_2** crossing to **Min S_2** a crossing point with the S_1 state is intercepted (**CI S_2/S_1 planar**), which is almost degenerate and geometrically very close to **Min S_2**.

Thus, a sudden and fully efficient depopulation to S_1 is expected through this point. Then, following the $S_2\rightarrow S_1$ hop, relaxation takes place on the lowest excited S_1 ($n\rightarrow\pi^*$) state and, finally, the planar *minimum* on this surface (**Min S_1**) is populated (see Figure 5).

In conclusion, according to this model, the final excited-state outcome of the initial multistate deactivation process is to populate the planar minimum (**Min S_1**) on the lowest singlet excited ($n\rightarrow\pi^*$) state $S_1(B_g)$, which thus acts as the collecting point of the photoexcited molecular population.

It is worth noting that this model is a Kasha-rule based picture of the process that, substantially, assigns to the lowest energy excited-state alone the leading role in dictating and controlling the photochemical behavior of the chromophore. Remarkably, the whole multistate relaxation path, from **FC** to **Min S_1**, is characterized by skeletal stretching deformations only, while no torsions are involved. That is, according to this Kasha rule-based model, it is through a planarity conserving motion (**FC→CI S_3/S_2→CI S_2/S_1** planar**→Min S_1**) that the system reaches the S_1 minimum starting from the FC region on a higher energy state. Since this process involves a *barrierless* route, it is predicted to occur in an ultrafast (subpicosecond) time scale.

The S_1/S_0 deactivation funnel (**CI S_1/S_0 90°**) can be accessed from **Min S_1** by overcoming a barrier on S_1 (**TS**) of 11 kcal/mol (see Figure 6): this radiationless decay and photoproduct formation route is unlikely to be very efficient, due to the high energy barrier involved (see also the discussion below). Thus, two other possible mechanisms for deactivation and ground-state recovery from **Min S_1** may become competitive, in principle: i) a radiative path (i.e., fluorescence, which has been computed to occur at 547 nm), and ii) a radiationless channel involving an inter system crossing (ISC) between S_1 and T_1 (which are almost degenerate at **Min S_1**) and, following relaxation on T_1, a back ISC to S_0 (a detailed description of triplet photochemistry will be provided below in a dedicated subsection).

In conclusion, the following computational evidence may be summarized for the static (i.e., Kasha rule-based) model (see Figure 7):

i) The photoexcited population (or at least most of it) is collected on **Min S_1** through a barrierless and ultrafast (sub ps) relaxation process that preserves the planarity of the system backbone.

ii) A barrier of 11 kcal/mol is involved on going from **Min S_1** to **CI S_1/S_0 90°**: that is, for this channel to be populated, energy leaking (i.e., vibrational energy redistribution) must take place to let the energy flow from the initially populated stretching modes to the torsional (reactive) modes. This process takes time (ps time scale at least). Additionally, the kinetic energy is redistributed not only to the reactive (central C═C bond) torsional mode, but it is dissipated on several other (unreactive) modes, which means that not all

Table 2. CASSCF(14,10)/ano-s and CASPT2/ano-s Energies of Fumaramide (E-1), Dimethyl-Fumaramide (E-2) and Tetramethyl-Fumaramide (E-3). All the States are Ordered by CASSCF Energy

Geometry/ symmetry		State	*E*-1 ΔE (kcal/mol) CASSCF[a]	*E*-1ΔE (kcal/mol) CASPT2[b] (ΔE *TD-DFT in parenthesis*)	*E*-2 ΔE (kcal/mol) CASPT2[b]	*E*-3 ΔE (kcal/mol) CASPT2[b]
FC	A_g	S_0	0.00	0.00	0.00	0.00
	B_g	S_1 ($n\pi^*$)	114.91	95.75 (90.39)	97.91	95.21
	A_u	S_2 ($n\pi^*$)	118.03	100.01 (94.55)	102.19	99.12
	B_u	S_3 ($\pi\pi^*$)	158.14	119.55 (117.38)	113.95	103.70
	A_g	S_4 ($\pi\pi^*$)	159.63	120.98 (117.61)	113.08	103.17
		T_1 ($\pi\pi^*$)	82.87	80.23	81.41	80.29
		T_2 ($n\pi^*$)	109.78	93.84	96.05	95.69
		T_3 ($n\pi^*$)	112.41	97.72	102.19	98.87
		T_4 ($\pi\pi^*$)	128.57	110.37	113.95	105.80
		T_5 ($\pi\pi^*$)	131.61	110.64	113.08	102.36
Min S_1		S_0	34.86	27.22		
		S_1 ($n\pi^*$)	79.84	79.52		
		S_2 ($n\pi^*$)	128.54	113.52		
		S_3 ($\pi\pi^*$)	134.55	111.73		
		S_4 ($\pi\pi^*$)	150.64	154.17		
		T_1 ($\pi\pi^*$)	75.56	76.8		
		T_2 ($n\pi^*$)	80.13	77.43		
		T_3 ($\pi\pi^*$)	126.85	108.98		
		T_4 ($n\pi^*$)	128.72	109.82		
		T_5 ($\pi\pi^*$)	154.90	127.87		
TS		S_0	77.72	73.02		
		S_1	88.64	90.42		
		S_2	146.43	138.73		
		S_3	148.86	122.90		
		S_4	156.16	153.76		
CI S_1/S_0 90°		S_0	82.30	73.98		
		S_1	85.24	81.18		
		S_2	152.38	129.17		
		S_3	154.66	142.43		
		S_4	165.07	150.38		
CI S_1/S_0 30°		S_0	106.97	97.89		
		S_1	110.67	99.88		
		S_2	173.37	163.11		
		S_3	207.69	160.97		
		S_4	223.01	181.49		
CI S_2/S_1planar		S_0	23.56	16.54		
		S_1	98.04	83.24		
		S_2	101.64	89.07		
		S_3	133.48	108.46		
		S_4	139.19	107.71		
High CI S_2/S_1		S_0	10.25	12.01		
		S_1	103.15	98.59		
		S_2	103.85	99.48		
		S_3	150.50	132.56		
		S_4	153.49	129.57		
Min S_3		S_0	18.08	7.26		
		S_1	99.24	74.60		
		S_2	103.46	81.37		
		S_3	136.53	104.03		
		S_4	139.30	106.85		
CI S_4/S_3		S_0	18.24	11.06		
		S_1	97.24	82.87		
		S_2	104.02	89.46		
		S_3	133.30	106.18		
		S_4	138.13	107.73		
CI S_3/S_2		S_0	24.97	23.02		
		S_1	92.82	82.70		
		S_2	117.93	98.54		
		S_3	127.45	99.59		
		S_4	152.50	119.79		
Min S_2		S_0	28.01	20.81		
		S_1	95.34	81.35		
		S_2	98.95	85.11		
		S_3	138.65	115.58		
		S_4	141.22	116.77		
Min T_1		S_0	55.75	55.24		
		S_1 ($n\pi^*$)	122.15	109.84		
		S_2 ($n\pi^*$)	123.19	112.90		
		S_3 ($\pi\pi^*$)	153.19	133.64		
		S_4 ($\pi\pi^*$)	154.77	135.23		
		T_1 ($\pi\pi^*$)	55.06	56.02		
		T_2 ($n\pi^*$)	121.53	110.85		
		T_3 ($n\pi^*$)	122.08	111.99		
		T_4 ($\pi\pi^*$)	152.79	133.78		
		T_5 ($\pi\pi^*$)	154.30	136.28		
TS S_0		S_0	55.26	56.47		
		S_1 ($n\pi^*$)	122.71	109.18		
		S_2 ($n\pi^*$)	123.93	110.95		
		S_3 ($\pi\pi^*$)	152.52	119.37		
		S_4 ($\pi\pi^*$)	154.88	120.66		
		T_1 ($\pi\pi^*$)	55.00	56.04		
		T_2 ($n\pi^*$)	121.22	112.20		
		T_3 ($n\pi^*$)	121.65	113.22		
		T_4 ($\pi\pi^*$)	152.99	135.39		
		T_5 ($\pi\pi^*$)	154.56	137.97		

[a] Fumaramide ground-state CASSCF/ano-s energy: −413.7670356036 au. [b] Fumaramide ground-state CASPT2/ano-s energy: −414.9076535320 au. Dimethyl-fumaramide ground state CASPT2/ano-s energy: −493.2672445046 a.u. Tetramethyl-fumaramide ground state CASPT2/ano-s energy: −571.6186677367 a.u.

the energy gets available for the photoisomerization process. This implies that this high-barrier channel must not be an efficient radiationless (i.e., fluorescence quenching) deactivation route, and that $\mathbf{S_1}$ depopulation may involve, in principle, other competitive deactivation mechanisms (such as emission or ISC, see the next two points).

iii) A radiative path, involving fluorescence at around 547 nm from **Min-S_1**, could in principle become competitive at these

Table 3. Quantum Yields and Ratios of Quantum Yields for Photoisomerization of Compounds **4** and **5** in Acetonitrile

Isomer pair	Direct irradiation			Sensitized[a]		
	$\phi_{E\rightarrow Z}$[b]	$\phi_{Z\rightarrow E}$[b]	$\phi_{E\rightarrow Z}/\phi_{Z\rightarrow E}$)	$\phi_{E\rightarrow Z}$	$\phi_{Z\rightarrow E}$	$\phi_{E\rightarrow Z}/\phi_{Z\rightarrow E}$)
4	0.044	0.044	1.05[c], 1.15[d], 0.99[e]	0.17	0.20	1.07[f], 1.18[e]
5	0.015	0.0028	5.27[c], 5.58[d], 5.36[e]	0.20	0.0008	37[f], 250[e]

[a] Using benzophenone as the sensitizer. [b] At 254 nm. [c] From the photostationary state composition upon 300 nm irradiation (Equation 1). [d] From the photostationary state composition upon 254 nm irradiation (Equation 1). [e] Determined directly from the quantum yields. [f] From the photostationary state composition.

conditions, but considering the low oscillator strength of the transition, it is unlikely to have a high radiative rate and this path will not play an important role.

iv) Also a competitive (fluorescence quenching) $S_1 \rightarrow T_1$ ISC may not be ruled out at **Min S_1**, since singlet and triplet are almost degenerate here and their spin−orbit-coupling (SOC) is significant (see the subsection below for a detailed discussion on triplet photochemistry).

Experiments support our hypothesis for an unfavored/inefficient photoisomerization process, the singlet photoisomerization quantum yield recorded for the threads **4** and **5** being rather small (see Table 3). On the other hand, emission is not observed and a very short (ps time scale) excited-state lifetime has been recorded for **3**-**6**, revealing that an efficient and ultrafast radiationless decay channel exists that quenches fluorescence and quickly triggers excited-state decay and reactant back formation. Although apparently rather surprising for a spin-multiplicity change event such as ISC (which generally implies longer timescales to occur), this process seems to be the unique way to account for the experimental data, provided it is ultrafast and very efficient. If this were the case, singlet and photosensitized (i.e., triplet) photochemistry should lead to the same outcome. That is, the recorded singlet photoisomerization quantum yields for the threads should coincide with the triplet values, since singlet photochemistry eventually turns out to become a triplet process. It is anticipated here that this is not the case: experimental results reported in Table 3 shows that the photoisomerization quantum yields recorded for the singlet and the triplet are very different.

Thus, while it can be concluded (according to the Kasha rule-based view) that **Min S_1** collects most of the excited population and that deactivation to S_0 must involve either emission or ISC, unfortunately neither of these mechanisms is supported by the experiments. This reasoning leads to the conclusion that fumaramide *is not a Kasha rule-based system*, i.e. its photochemistry cannot be accounted for dealing with the lowest energy points of each electronic state only. For a more correct and realistic interpretation of the experimental results nonstatic effects need to be accounted for, i.e. it is mandatory to explore also higher energy regions along (or close to) the MEPs and the crossing seams, which may turn out to become important for dynamics and will be the focus of the *dynamic model* presented below.

(B) The Dynamic Model. The inconsistencies found between the experiments and the Kasha rule based-model reported in the previous section, motivated us to explore higher energy regions of the photochemically relevant potential energy surfaces in order to identify other feasible deactivation mechanisms. The low isomerization quantum yields observed in the singlet photochemistry suggest that deactivation must involve funnel regions where the C═C central bond is not yet fully twisted, so that reactant back formation on the ground-state surface becomes the favored process. Furthermore, the absence of fluorescence, the ps excited-state lifetime and the different singlet and triplet quantum yields observed, reveal that a direct efficient radiationless decay channel from S_1 to S_0 exists (that is, this route does not involve the triplet state, i.e. no ISC occurs). Starting from these premises, we have investigated the intersection space between S_0 and S_1, performing series of constrained conical intersection optimizations at different values of the central C═C bond twisting angle. Thanks to this procedure, we have identified an extended S_1/S_0 crossing seam which spans structures of increasing energy from 90° (i.e., the fully twisted and lowest energy **CI S_1/S_0 90°**) to 150° (**CI S_1/S_0 30°**, possessing an almost planar backbone), see Figure 8.

Analogously, an extended crossing seam exists also between S_2 and S_1. In particular, we have identified another crossing between S_2 and S_1 (**High CI S_2/S_1**) that has a planar structure, yet is much higher in energy then **CI S_2/S_1 planar**. Remarkably, this crossing has the same energy as **CI S_3/S_2** and it is close to this (2.85 mass weighted a.u. distance only, see Figure 9). This means that the S_2/S_1 crossing space spans a region of increasing energy (and substantially planar structures) that approach the high energy part of the S_2 MEP. It is thus conceivable that high energy regions of the S_2/S_1 crossing seam (such as the planar **High CI S_2/S_1**) becomes accessible from **CI S_3/S_2** (i.e., from the beginning of the S_2 MEP) for dynamics reasons: even normal (thermal) vibrations may easily drive the system into the S_2/S_1 crossing space from the top of the S_2 MEP. Hence, the system does not necessarily need to fully follow the S_2 MEP till to the S_2 minimum to hit the S_2/S_1 crossing seam and hop to S_1, since this process (i.e., the radiationless decay to S_1) can occur much earlier than predicted previously by the static (Kasha rule-based) model. If that occurred, as it appears from these analysis, then the system could jump to S_1 at a much higher energy than **CI S_2/S_1 planar**, thus accessing novel high energy regions of the S_1 PES such as the high energy (almost planar) structures of the S_1/S_0 intersection space previously shown (see Figures 8 and 9).

In conclusion, it is conceivable that the system decays to high energy regions of S_1 via S_2/S_1 crossing points nearby the planar and high energy **High S_2/S_1 CI** found close to the **CI S_3/S_2**, and that from here it hits the S_1/S_0 crossing seam (and, therefore, it is funneled to S_0) much before reaching the twisted CI minimum (**CI S_1/S_0 90°**): i.e. deactivation to S_0 may occur via high energy almost planar (or only slightly twisted) S_1/S_0 CI structures. If this were the case, besides opening a very efficient radiationless decay channel to S_0 that quenches the fluorescence, a very small photoisomerization quantum yield would be expected, since reactant back formation (following decay from almost planar molecular structures) would be the most favored event. A schematic representation of this behavior is reported and summarized in Figure 10.

This "dynamic interpretation" of fumaramide deactivation can be schematically represented by using two bidimensional intersecting surfaces as models for the S_1 and S_0 PES (see Figure 11). The *x*-axis represents the relevant stretching coordinate and the *y*-axis the rotation of the central C═C bond. It is apparent that an extended crossing seam exists between these two surfaces even for small torsional angles, although at higher energies. Thus, if the system may hit these regions, it can hop down to S_0 before reaching the *minimum* on S_1. Under this hypothesis, it comes clear why no emission is observed. Moreover, the low photoisomerization quantum yield observed is a consequence

Table 4. Fumaramide Bond Distances (Å)

Bond	Geometries										
	FC	Min S_1	TS	CI S_1/S_0 90°	CI S_1/S_0 30°	Min S_2	CI S_2/S_1 planar	CI S_2/S_1 High	CI S_3/S_2	Min T_1	Min S_3
C1−C2	1.340	1.409	1.482	1.474	1.460	1.418	1.427	1.461	1.458	1.466	1.430
C1−C3	1.492	1.359	1.330	1.349	1.376	1.396	1.403	1.418	1.370	1.471	1.413
C2−C4	1.492	1.471	1.473	1.478	1.507	1.396	1.397	1.416	1.458	1.470	1.413
O1−C3	1.207	1.368	1.365	1.324	1.352	1.284	1.288	1.294	1.346	1.210	1.273
O2−C4	1.207	1.209	1.209	1.209	1.198	1.284	1.284	1.271	1.215	1.209	1.273
N1−C3	1.359	1.390	1.388	1.384	1.378	1.362	1.364	1.349	1.339	1.372	1.350
N2−C4	1.359	1.377	1.379	1.377	1.349	1.362	1.372	1.375	1.368	1.378	1.350

of the substantially planar molecular geometries (i.e., small rotation of the central C═C bond) of the S_1/S_0 crossings that trigger the decay to the ground-state and promote reactant back formation.

Fairly stated, a computational validation of this model would require a systematic dynamical investigation by performing trajectories computations (anyway, a simple experiment is suggested - see section 3.4 below - that may be alternatively used to validate this mechanistic scheme). Although this is out of the scope of this work (CASPT2 dynamics is not affordable even for such a small system), it is worth noting that this non-Kasha rule behavior does characterize the photochemistry of other organic chromophores, such as azobenzene[40,41] and its derivatives. For instance, cyclohexenylphenyldiazene (a simple surrogate of the azobenzene photochromic unit) has been recently investigated, that show a very similar (Kasha rule breaking) photophysical scheme.[40] This would represent the second example where such a mechanistic model applies.

Finally, it must be noted that no side products have been detected in these simulations, which accounts for the effectiveness of the photoactive fumaramide unit as its photoisomerization can be repeated indefinitely without losses due to side reactions. In particular, excited-state relaxation channels involving amide bond rotations (which may be a potential source of side reactions and may produce different isomers as side photoproducts if different nitrogen substituents are present) turn out to be unfavored processes (see end section S1 of the Supporting Information for a detailed discussion).

E⇆Z Photoisomerization by Triplet Sensitization. In order to explore the reactivity on the lowest triplet state T_1 ($\pi\pi^*$), the *E*⇆*Z* photoreaction of threads **4** and **5** has been studied by using a series of triplet photosensitizers, and the isomerization quantum yields with benzophenone have been recorded and collected in Table 3. Figure 12 shows the extent of conversion to the *Z*-isomer after prolonged irradiation of the *E*-isomers of **4** and **5** in the presence of sensitizers of different triplet energies. For very low sensitizer energy, conversion does not occur, but when the triplet energies are high enough, photostationary states are obtained. The experimental energy gap recorded in the thread **4** between S_0 and T_1 is 67 ± 2 kcal/mol (the vertical triplet energies are probably higher, see also the discussion below), while the onset of conversion occurs at 59 kcal/mol for **5**, and at 65 kcal/mol for **4**. For a range of triplet energies, *E*-**5** can be almost quantitatively converted to its *Z*-isomer. This is because the vertical triplet energy of *Z*-**5** is sufficiently higher that the sensitizer can only transfer its energy to the *E*-isomer, which is thus effectively depleted. A similar situation is found for many conjugated alkenes[24] when the *E*-isomer has a planar chromophore, but the sterically more crowded *Z*-isomer is twisted at the C−C single bonds. Interestingly, this situation does not apply to the case of the threads **4**, in which the photostationary state has roughly equal amounts of both isomers. This is due to the fact that *Z*-**4** adopts a planar structure, with an internal hydrogen bond. As a result, the triplet energies of *E*-**4** and *Z*-**4** are not very different, and selective energy transfer is not possible. The situation is illustrated in Figure 13 (that reports results from B3LYP/6−31G* calculations), using compounds **2** and **3** as models for **4** and **5**, respectively.

Computational Analysis of the Isomerization in the Triplet T_1 State: S_1-T_1 and T_1-S_0 Inter-System Crossings. Our calculations (at both CASPT2 and B3LYP level) predict a higher (ca. 80 kcal/mol, see Table 2 and Figure 13) vertical (FC) S_0-T_1 energy gap than the recorded (67 ± 2 kcal/mol) experimental value. It is reasonable to associate the latter value to the energy difference between the planar ground-state minimum and the relaxed planar structure on the triplet T_1 surface (called $0-0_{planar}$ thereafter). Very remarkably, the computed singlet−triplet $0-0_{planar}$ energies for *E*-**2** and *E*-**3** (65.9 and 61.9 kcal/mol respectively, see Figure 13) match fairly well with the experimental value recorded for the threads (note that compounds **2** and **3** are used as models for threads **4** and **5**, respectively). Since our computations in vacuo closely reproduce the spectroscopic data recorded in solution, solvent effects do not play a major role in this specific case and the isolated system should represent an accurate model of the photochemical behavior in solution.

The T_1 wave function is characterized by a single-electron occupation of the *HOMO* (π) and *LUMO* (π^*) orbitals on the central double bond (orbitals 7 and 8, see Figure 1). As a consequence, a strong weakening of the central C═C double bond is expected in this state and, consistently, geometry optimization on T_1 leads to a 90° twisted central double bond minimum (**Min T_1**, see Figure 14). This is a recurring property of many olefinic systems (e.g., ethylenes, stilbenes, azobenzenes, etc)[40,41] in their lowest triplet ($\pi\pi^*$) state.

Interestingly, besides the usual sensitization process, T_1 can be populated by intersystem crossing (ISC) from the S_1 minimum (**Min S_1**). In fact, S_1, T_2 ($n\pi^*$) and T_1 ($\pi\pi^*$) are substantially degenerate at this point (the three states are within 2.5 kcal/mol, see Figure 14 and Table 2). Additionally, the computed spin−orbit-coupling (SOC) between $T_1(\pi\pi^*)$ and $S_1(n\pi^*)$ is quite large (28 cm^{-1}) at **Min S_1**, suggesting that $S_1 < 199 \gg T_1$ ISC can be very efficient and fast (ps time scale, see also the discussion below). Furthermore, constrained geometry optimizations on T_1 at different twisting angles of the central C═C bond show that a wide region around **Min T_1** (between 70° and 100° of twisting) exists (Figure 14) where the PES of T_1 and S_0 are substantially degenerate. Although T_1-S_0 SOC values are rather small along the twisting mode in this region (ca. 0.02 cm^{-1}, see Figure 14), an out of plane mode

(40) Conti, I.; Marchioni, F.; Credi, A.; Orlandi, G.; Rosini, G.; Garavelli, M. *J. Am. Chem. Soc.* **2007**, *129*, 3198.
(41) Cembran, A.; Bernardi, F.; Garavelli, M.; Gagliardi, L.; Orlandi, G. *J. Am. Chem. Soc.* **2004**, *126*, 3234.

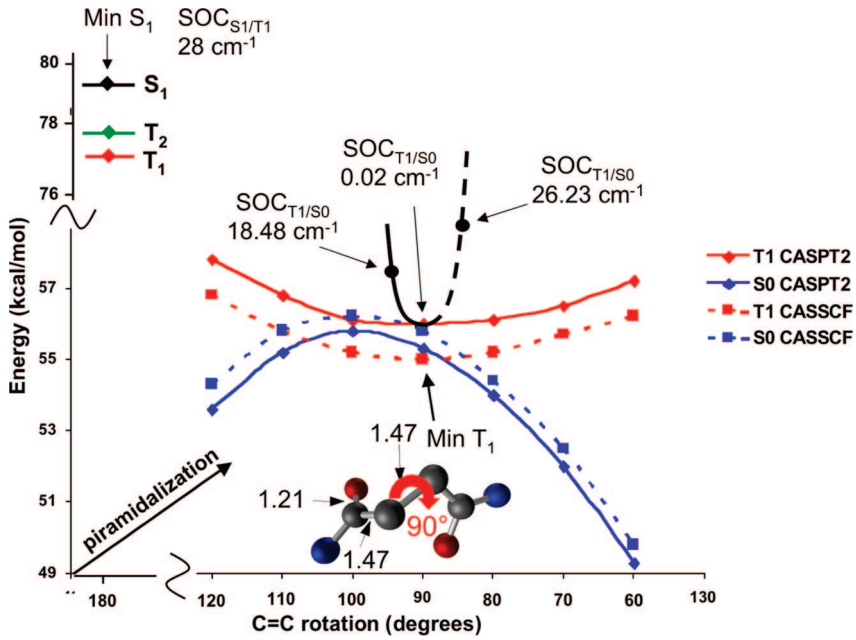

Figure 14. T_1 and S_0 energy profiles along the central bond twisting coordinate for the region surrounding the triplet twisted minimum (**Min T_1**): constrained CASSCF/6−31G* geometry optimizations followed by single point CASPT2/ano-s corrections are used for this purpose. The energies of S_1, T_2 and T_1 at the **Min S_1** geometry are reported on the left up side. Computed SOC values are also reported in italic. The vibrationally activated $T_1 \sim > S_0$ ISC in the **Min T_1** region is also displayed: pyramidalization at the carbonyl carbon C3 (C4) is the orthogonal vibrational mode that triggers $T_1 \sim > S_0$ ISC by enhancing T_1-S_0 SOC values.

of 730 cm^{-1} exists that involves the asymmetric pyramidalization of the carbonyl carbons C3 (C4) and leads to large T_1-S_0 SOC values: according to our computations, zero point energy oscillations for this mode already lead to SOC values up to ca. 30 cm^{-1} (see Figure 14). Thus, it is apparent that another efficient and ultrafast (ps time scale) ISC from T_1 to S_0 that is activated vibrationally, can easily occur in the twisted region around **Min T_1**. It is suggested here that the slower (19 ps) decay component observed in fumaramides singlet photochemistry (see the discussion above about time-resolved spectroscopic data) is related to this triplet T_1 channel and can be assigned to its population ($S_1 \sim > T_1$) and/or decay ($T_1 \sim > S_0$), see Figure 10. Although these ISC processes may appear surprisingly fast (spin-multiplicity change events generally implies longer timescales to occur), a similar behavior has been recognized in other olefinic chromophores (e.g., ethylenes, azobenzenes, etc),[40,41] that, as mentioned above, display a very similar T_1/S_0 topology with a very efficient and ultrafast (ca. 10 ps time scale) $T_1 \sim > S_0$ ISC (see also the discussion in the following subsection). This argument nicely supports the previous assignment for T_1 being responsible of the 19 ps decay component observed in *E*-**4**, as it well matches with the time scale of these ISC processes. Additionally, the very short T_1 lifetime implies a difficult spectroscopic detection of this state and well accounts for the lack of spectroscopic observations of T_1 in fumaramides.

Interpretation of Photoisomerization Quantum Yields in the Triplet State. The experimental quantum yield observed for the photosensitized isomerization of the threads is about 1 order of magnitude higher than the one recorded in the singlet (see Table 1). Remarkably, this higher value is in agreement with our results that show that the triplet T_1 state crosses (and is degenerate with) the ground-state in the twisted region and that the path to this twisted region is barrierless (Figure 14). In fact, these findings support the idea that the decay of T_1 can occur more efficiently via the torsion mechanism with a rate depending on the strength of the relevant spin−orbit-couplings similarly to what reported for other olefinic chromphores such as stilbenes and azobenzenes.[40,41] Specifically, in our previous works on azobenzene[41] and cyclohexenylphenyldiazene[40] (which, as mentioned above, present a similar T_1/S_0 topology with degenerate S_0 and T_1 states at the twisted structures), we have demonstrated that SOC values of ca. 20 cm^{-1} (which are of the same magnitude as the ones computed here for fumaramide, see the discussion above and Figure 14) are large enough to ensure that the rate of the $T_1 \sim > S_0$ ISC process is of the order of 10^{11} s^{-1}. This rate indicates that the system can decay from T_1 to the ground-state in a ca. 10 ps time scale and that torsion provides indeed a very efficient mechanism for the T_1 decay and isomerization. Thus, a situation similar to that found in azobenzene[41] and cyclohexenylphenyldiazene[40] is suggested here for fumaramide, which should lead to a very short (i.e., ps time scale) T_1 lifetime in agreement with the difficult spectroscopic detection of this state.

In conclusion, a more efficient isomerization of the central double bond (than in the singlet state) is expected through this route. Indeed, this is what recorded photoisomerization quantum yields reveal. Finally, the existence of an extended T_1/S_0 degenerate region that starts from ca. 70° to ca. 100° of central C═C bond twisting (see Figure 14) well explains why the observed triplet quantum yields are less than 0.5: as the degenerate region is first encountered on the reactant side (i.e., before 90° fully twisted structure), an ISC leading mainly to reactant back formation is always expected, as the experiments reveal indeed.

3.3. Dynamics vs Static Control of the Photochemical Process. It would be highly rewarding if the *dynamics* vs the *static* model could be tested and proved experimentally. The key point for such an experiment would be the possibility to pump directly to the S_1 state (which is symmetry forbidden) with a small and controlled amount of (excess) vibrational energy such as hitting a vibronic level that can borrow intensity by Herzberg−Teller mechanism. This would populate selec-

tively the S_1 minimum region, and leave no energy available for activation of the radiationless decay channel to the twisted CI (**CI S_1/S_0 90°**). Under such conditions, which would bias a Kasha rule-controlled system, emission and/or ISC could in principle become competitive, as already discussed in subsection 3.2 above. If this were the case, emission might be observed. Alternatively, if ISC occurs and is a competitive and efficient process (as we indeed expect to be, see subsection 3.3 above), singlet photochemistry will turn out to become a triplet process and the same photoisomerization quantum yield observed in photosensitized experiments should be recorded also for singlet photochemistry. This would represent a novel and intriguing aspect of fumaramide-based photocontrolled molecular devices, which may be suitably exploited to tailor their photochemical properties and reactivity as a function of the technological applications pursued. However, impeded by the small absorption cross section of the S_1 state, such experiments have as yet not been successful.

4. Conclusions

A computational investigation of fumaramide photochemistry (as a model of fumaramide threads) jointly to photochemical and time-resolved spectroscopic measurements on fumaramide/maleamide compounds revealed a complex multistate photophysics of this photoactive unit, opening several intriguing scenarios. We have identified a pattern of possible deactivation mechanisms that may involve, in turn, internal conversion, intersystem crossing or emission. These are all based on the analysis of the *minimum* energy paths computed on the PESs of the photochemically relevant excited states (which are supposed to drive the relaxation of the excited molecules) and the crossing seams between them (which are thought to trigger radiationless decay). For the fumaramide unit in vacuo, it has been shown that a static (i.e., Kasha rule based) interpretative model (where **Min S_1** acts as the collecting point of the photoexcited population) does not account for all the experimental evidence, while a dynamic picture (involving decay to S_1 and S_0 at higher energy regions of the crossing seams) may easily explain all the observations recorded for fumaramide compounds in solution. This provides a solid computational evidence for fumaramide not being a Kasha system (i.e., Kasha rule is violated).

This is not the first example of Kasha rule failure: azobenzene and related systems (such as the phenylazocyclohexene) behave the same, as it has been previously shown by both experimental and theoretical works.[40,41] Nevertheless, fumaramide provides a very interesting case because it is a small molecule that can be studied using very accurate high level ab initio methods, which provide a precise and reliable picture of its photochemistry. Furthermore, it is also the base of an important family of photoresponsive nanodevices such as the rotaxane shown in Scheme 1.[16,18] In this respect, it is worth noticing that fumaramide photochemistry does not involve efficient side reactions, so that it can be operated continuously under illumination with very little loss, which makes it a very effective photoactive unit in nanodevices.

Our study also suggests a way to operatively achieve a static or dynamics control of the photochemistry of this system, thus switching on between two 'modes' that lead to different photochemical outcomes (i.e., different photoisomerization quantum yields, excited-state lifetimes, etc). From a computational standpoint, full quantum-mechanic nonadiabatic molecular dynamics computations will have to be used to quantitatively investigate this issue and access the importance of nonequilibrium (i.e., dynamics) effects along the relaxation process. This will be to topic of future investigations. Nevertheless, the static description of the PESs shown here provides a rationale for fumaramide photochemistry, both in the singlet and triplet manifold, that accounts for the observations recorded in the isolated threads.

In conclusion, a rationale for the spectroscopic properties, photoisomerization quantum yields and lifetimes observed in the direct (i.e., singlet) irradiation experiments has been provided, and a model for the sensitized (i.e., triplet) photochemical reactivity as been drawn that accounts for the different behavior (e.g., different isomerization quantum yields) observed in the threads.

Acknowledgment. The support by funds from Bologna University (Progetti Strategici d'Ateneo 2005: Progetto CompRenDe) is gratefully acknowledged. We thank CINECA and INSTM for granted calculation time. Part of this work has been supported by the European Union project STAG (STRP 033355), and The Netherlands Organization for the Advancement of Research (NWO). Dr. Bert Bakker synthesized *N*,*N*,*N*′,*N*′-tetramethylfumaramide.

Supporting Information Available: Conformational analysis (section S1), electronic absorption spectroscopy (section S2), irradiation experiments (section S3), complete references[26] and[29] (section S4), Cartesian coordinates of all the optimized structures discussed in the text (section S5), one table for the triplet sensitization experiments (Table S1) and two figures (Figure S1 and S2). Complete refs 26 and 29. This material is available free of charge via the Internet at http://pubs.acs.org.

JA802531J